Physics Letters A 384 (2020) 126187

Contents lists available at ScienceDirect

Physics Letters A

www.elsevier.com/locate/pla

Anisotropic collapse in three-dimensional dipolar Bose-Einstein condensates

Boaz Ilan *, Jessica Taylor

Applied Mathematics Department, University of California, Merced, 5200 North Lake Rd., Merced, CA 95343, USA

ARTICLE INFO

Article history:
Received 15 July 2019
Received in revised form 30 November 2019
Accepted 2 December 2019
Available online 6 December 2019
Communicated by B. Malomed

Keywords:
Nonlocal NLS equation
Supercritical collapse
Davey-Stewartson system

ABSTRACT

We study the (3+1)-dimensional Gross-Pitaevskii / Nonlinear Schrödinger equation describing a dipolar Bose-Einstein condensate. Bound states are computed using accurate numerical techniques. When the dipolar strength is negative, the total number of atoms *vs.* frequency relationship for these bound states is multi-valued and possesses a cusp point, which corresponds to a "candlestick" ground state. Direct simulations of this ground state exhibit strongly-anisotropic collapse of its nucleus, with different contraction rates along the dipole axis and perpendicular to it. We propose an anisotropic self-similar theory to explain this dynamics. The physical implications are discussed.

Published by Elsevier B.V.

1. Introduction

Self-similarity and singularity formation are two fascinating phenomena of wave dynamics. Nonlinear dispersive waves can exhibit both in the form of self-similar collapse [1–3]. Self-similar collapse has been studied and observed in a variety of physical systems, such as laser propagation in plasma [4,5], laser propagation in optical-Kerr media [6], and surface gravity waves in fluids [7]. One of the universal equations in nonlinear wave theory is the nonlinear Schrödinger (NLS) equation and its generalizations. The possibility of collapse and its rate depend on the spatial dimension. For the focusing cubic NLS equation in $(d+1)$-dimensions, there is a critical dimension, $d=2$, such that collapse is possible only when $d \geq 2$. Thus far, the theory of singularity formation is well-developed in the critical case [1,3]. In the supercritical case $(d>2)$ it is known that the mass in the collapsing region diminishes to zero during the collapse process, a phenomenon termed "weak collapse". However, the theory is much less developed in supercritical case. In addition, there have been few detailed studies of collapse dynamics in anisotropic NLS equations.

Bose-Einstein condensates (BECs) provide new ways for studying ultracold dispersive matter waves [8,9]. BECs can undergo collapse, which has been observed in many experiments, cf. [10–12]. BEC collapse may also be related to gravitational collapse [13,14]. BECs offer a natural system to study supercritical collapse dynamics, since their mean-field is described by a (3+1)D Gross-Pitaevskii (GP) or NLS equation. For example, weak collapse was recently observed in an isotropic BEC [15]. Transition-metal BECs, such as those using ^{52}Cr or ^{168}Er atoms, exhibit strong dipole-dipole interactions [8]. The experiments of Lahaye et al. provided the first observations of collapse in dipolar BECs and predicted its anisotropic nature [16], which they observed shortly thereafter [17] in the form of d-wave collapse. Anisotropic collapse in dipolar BECs was also reported in [18]. In reality, singularity is always arrested by some mechanism, cf. [16]. However, a deeper understanding the nature of collapse can provide insight into this complex dynamics.

Motivated by these experimental and theoretical studies, we study computationally the anisotropic collapse dynamics in a (3+1)D dipolar NLS equation. We compute the bound states (structure functions) and study their kinetic properties.

2. Preliminaries

The dynamics of the mean-field wavefunction, $\psi(\boldsymbol{r},t)$, of a dipolar BEC can be described by a nonlocal generalization of the NLS equation [8,9],

$$i\hbar\psi_t = \left(-\frac{\hbar^2}{2m}\Delta + V_{\text{ext}}(\boldsymbol{r}) + \frac{4\pi\hbar^2 a_s}{m}|\psi|^2 + U_{\text{dip}} * |\psi|^2\right)\psi\ , \tag{1}$$

where m is the mass of the boson, $\boldsymbol{r}=(x,y,z)$ is the position variable in $\mathbb{R}^3$, $\Delta = \partial_{xx}^2 + \partial_{yy}^2 + \partial_{zz}^2$ is the 3D Laplacian, $V_{\text{ext}}(\boldsymbol{r})$ is

* Corresponding author.
E-mail address: bilan@ucmerced.edu (B. Ilan).

https://doi.org/10.1016/j.physleta.2019.126187
0375-9601/Published by Elsevier B.V.

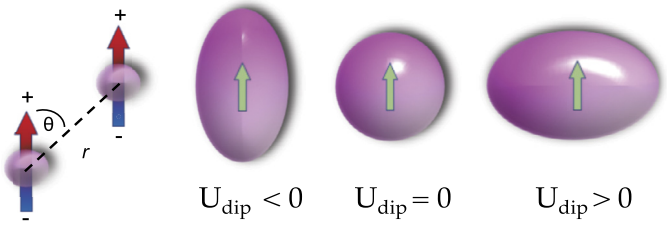

Fig. 1. For a prolate condensate (elongated along the z axis), most dipoles are aligned with the negative side of one atom near the positive side of another atom. In this case the overall effect of dipole-dipole interactions is attractive. The situation is reversed when the condensate is oblate. Thus, dipolar effects [U_{dip} defined in Eq. (2)] can vary dynamically between attractive and repulsive depending on the shape of the condensate.

an external potential, a_s is the short-range boson-boson scattering length, and the last term models long-range dipolar interactions, where the symbol $*$ denotes convolution in $\mathbb{R}^3$ with the dipolar potential

$$U_{\text{dip}}(\boldsymbol{r}) = \frac{C_{dd}}{4\pi}\frac{1-3\cos^2\theta}{|\boldsymbol{r}|^3}\,, \tag{2}$$

where θ is the angle relative to the dipole axis (which we take to the z axis) and C_{dd} is the strength of the dipolar interactions. We consider (9) with the anisotropic harmonic trapping potential

$$V_{\text{ext}}(\boldsymbol{r}) = V_0\left[x^2+y^2+(\kappa z)^2\right]\,, \tag{3}$$

where V_0 is the potential depth and κ is the anisotropy (aspect-ratio) parameter. $\kappa<1$ and $\kappa>1$ correspond to a prolate (cigar-shaped) and oblate (pancake-shaped) potentials, respectively.

The short-range interactions can be tuned between repulsive ($a_s>0$) or attractive ($a_s<0$) using a Feschbach resonance. The dipolar interactions can straddle the continuum between attractive and repulsive effects, depending on the shape of the condensate – see Fig. 1. Typically, $C_{dd}>0$, as was the case in the experimental study [17] and as is assumed in Fig. 1. In this case, for dipoles polarized along the long axis of a prolate BEC ($\theta\approx 0$), $U_{\text{dip}}<0$ and the overall contribution of the dipolar interactions is attractive because the dipoles are aligned head-to-toe. On the other hand, for dipoles polarized along the short axis ($\theta\approx\frac{\pi}{2}$) of an oblate BEC, $U_{\text{dip}}>0$ and the overall contribution of the dipolar interactions is repulsive because the dipoles repel each other. Note that, as our results demonstrate, the condensate's shape can be oblate even when it is trapped in a prolate potential.

On the other hand, it has been predicted that by tilting the polarization off-axis and rotating it rapidly, the resulting time-averaged dipolar interactions give rise to an *effective* $C_{dd}<0$ [19]. In that case, the situation is reversed in the sense that a prolate-shaped condensate can give rise to repulsive dipolar effects. This is the case we study.

2.1. Alternate form of the equations

After standard normalizations (cf. [8]), Eq. (1) takes the form

$$i\hbar\psi_t = \left(-\frac{1}{2}\Delta + V_{\text{ext}}(\boldsymbol{r}) + g_1|\psi|^2 + g_2\tilde{U}_{\text{dip}}*|\psi|^2\right)\psi\,, \tag{4}$$

where g_1 is the short-range interaction constant, g_2 is the dipolar constant, and[1]

$$\tilde{U}_{\text{dip}}(\boldsymbol{r}) = \frac{3}{4\pi}\frac{1-3\cos^2\theta}{|\boldsymbol{r}|^3}\,. \tag{5}$$

[1] The coefficient 3 is chosen for convenience.

This is equivalent to normalizing the physical variables to the characteristic nonlinear length scales of the system, which are determined by the atomic scattering lengths [8]. Two conserved quantities of (4) are the total number of atoms (mass) and energy (Hamiltonian), given respectively by

$$N[\psi] = \int_{\mathbb{R}^3}|\psi|^2\,d\boldsymbol{r} \tag{6}$$

and

$$E[\psi] = \int_{\mathbb{R}^3}\left\{\frac{1}{2}|\nabla\psi|^2 + V_{\text{ext}}|\psi|^2 + \frac{1}{2}g_1|\psi|^4 + \frac{1}{2}g_2\tilde{U}_{\text{dip}}*|\psi|^2\right\}|\psi|^2\,d\boldsymbol{r}\,. \tag{7}$$

These quantities are useful for our analysis of the bound states and collapse dynamics. We remark that many studies choose to normalize the wavefunction such that $N[\psi]=1$, but we choose not to do this, because we are interested studying the bound states as the number of atoms vary.

It is useful to recast Eq. (4) in a different form. To do so we use an alternative expression for the dipolar potential (5) (cf. [8]),

$$\frac{3}{4\pi}\frac{1-3\cos^2\theta}{|\boldsymbol{r}|^3} = -\delta(\boldsymbol{r}) - \frac{3}{4\pi}\frac{\partial^2}{\partial z^2}\left(\frac{1}{|\boldsymbol{r}|}\right)\,, \tag{8}$$

where δ stands for the Dirac delta function. Substituting (8) into (4), observing that the r^{-1} potential on the right-hand side of (8) is proportional to the kernel of the Laplace operator in $\mathbb{R}^3$, and introducing the field φ yields the coupled system

$$i\psi_t = \left\{-\frac{1}{2}\Delta + V_{\text{ext}}(\boldsymbol{r}) + (g_1-g_2)|\psi|^2 + 3g_2\varphi_{zz}\right\}\psi\,, \tag{9a}$$

$$\Delta\varphi = |\psi|^2\,. \tag{9b}$$

System (9) (with $V_{\text{ext}}=0$) resembles the one derived by Benney and Roskes [20] for the propagation of surface water waves over a deep bottom coupled to a slowly-varying mean field (the average water depth). In analogy, for a dipolar BEC, φ describes a slowly-varying electrostatic potential driven by the local density of the bosons, $|\psi|^2$. We remark that a similar looking system arises in the study of surface water waves [20], commonly known as the Davey-Stewartson system [21]. In contrast to BECs, in water waves the surface has two spatial dimensions. This dimensional distinction has significant consequences on the possibility of singularity formation. In particular, the 2D case (as in water waves) is a critical dimension for collapse, whereas, for a 3D BEC, the resulting system is supercritical. Moreover, this also has significant consequences on the collapse dynamics. In particular, it was shown in [22] that the solutions of the 2D Davey-Stewartson system can undergo *mildly anisotropic* collapse, where the collapsing region is self-similar to the ground state. In contrast, as we show below, solutions of (4) can undergo *strongly anisotropic* collapse.

2.2. Instability regions and collapse

Intuitively, for collapse to occur in a dipolar BEC, either the local and / or the dipolar interactions need to be attractive. However, as noted above, there is no simple criterion to determine when the dipolar interactions are attractive. In general for NLS-type equations, there are conditions that sufficient for collapse and there are conditions that are necessary for collapse, but there are no conditions that are both necessary and sufficient for collapse [3]. Moreover, the theory of collapse is far less developed for supercritical NLS equations, to which (3+1)D System (9) belongs.

Lushnikov [23,24] obtained sufficient criteria for collapse of solutions of System (9) in the case $g_1 < 0$ (attractive local interactions) and $g_2 > 0$. Those criteria, which were derived based on a generalized Virial Theorem, depend on whether the energy is below a certain critical threshold as well as the width (mean-square radius) of the initial wavefunction.

Carles et al. [25] and Antonelli and Sparber [26] obtained necessary conditions for collapse (or sufficient conditions for global existence). These studies identify two distinct *Unstable Regions*[2]:

- Unstable Region I:

$$g_2 > 0 \quad \text{and} \quad g_1 < g_2 \,. \tag{10}$$

- Unstable Region II:

$$g_2 < 0 \quad \text{and} \quad g_1 + 2g_2 < 0 \,. \tag{11}$$

Unstable Region I requires attractive local interactions ($g_1 < 0$). Unstable Region II requires sufficiently strong and attractive dipolar interactions. Unstable Region II suggests that collapse may occur even with repulsive local interactions. If this happens, it can be said that the collapse is due largely to the dipolar interactions. We are chiefly interested in Unstable Region II, which has not received much attention. Specifically, we focus on parameters that are inside Unstable Region II ($g_1 = 1$ and $g_2 = -1$) and also explore parameters that are at the borderline of this region ($g_1 = 1$ and $g_2 = -0.5$). It should be recapped that these conditions are only necessary for collapse.

3. Bound states and ground states

Based on thermodynamic arguments, a BEC is formed in an energetic ground state [8]. Moreover, the possibility of singularity formation in NLS-type equations is closely-linked to the existence of ground states [27]. For these reasons, it is useful to study the kinetic properties of the ground states of System (13). Assuming a time-harmonic solution,

$$\psi(\boldsymbol{r}, t) = u(\boldsymbol{r}) e^{-i\mu t} \,, \tag{12}$$

where μ is called the chemical potential (or frequency), leads to the coupled system of equations for a bound state $u(\boldsymbol{r})$,

$$\mu u = \left\{ -\frac{1}{2}\Delta + V_{\text{ext}}(\boldsymbol{r}) + (g_1 - g_2)|u|^2 + 3g_2\varphi_{zz} \right\} u \,, \tag{13a}$$

$$\Delta\varphi = |u|^2 \,, \tag{13b}$$

subject to $|u(\boldsymbol{r})| \to 0$ as $|\boldsymbol{r}| \to \infty$. System (13) is nonlinear and elliptic. In general, it admits infinitely many solutions. The standard characterization of a ground state (if it exists) is a bound state that minimizes the energy (7) subject to a fixed total number of atoms (6), *i.e.*,

$$u_{\text{gs}}(\boldsymbol{r}; \mu) = \arg\min \left\{ E[u] \;\middle|\; u \in H^1(\mathbb{R}^3),\ \|u\|_2^2 = N \right\} \,. \tag{14}$$

Once a bound state is found, μ and can be recovered from the relation

$$\mu = E[u] + \frac{1}{2}\int \left\{ g_1|u|^2 + g_2 U_{\text{dip}} * |u|^2 \right\} |u|^2 \, d\boldsymbol{r} \,. \tag{15}$$

In this formulation the chemical potential μ depends implicitly on N.

[2] Accounting for a different normalization constant in Eq. (5).

Existence and uniqueness of ground states of System (13) were studied in [26,28,29]. These studies proved that ground states exist and are unique in the two unstable regions defined above. We note that in [26,28], instead of using Definition (14), the ground states were characterized using the Weinstein functional, which has the advantage of being scaling-invariant. In [29] it was also observed analytically that the trapping potential plays a key role in stabilizing the ground states.

We also note the anisotropic collapse in generalized NLS-type equations with fourth-order dispersion were studied in [30]. In [31] the initial stage of anisotropic ring-type collapse in NLS equations was studied using a nonlinear Geometrical Optics approach.

4. Computational methods for bound states

Almost all theoretical studies of dipolar BECs bound states have used the Variational Method (Lagrangian averaging), pseudo-potentials, or similar techniques to reduce the 3D problem (13) to lower-dimensional approximations, cf. [24,32–41]. However, as noted above, singularity formation is sensitive to the dimensionality of the problem. Bao et al. developed a non-uniform spectrally accurate gradient flow method for computing the ground states of System (9) [42–44] Here we adapt the Accelerated Imaginary-Time Evolution Method (A-ITEM) [45], which is a uniform grid FFT-based gradient-flow method. As the problem is axi-symmetric, the bound states are functions of $(r_\perp, z)$, where

$$r_\perp = \sqrt{x^2 + y^2} \,. \tag{16}$$

We use this symmetry and employ the quasi-discrete Hankel transform [46] along $r_\perp$ and FFT along z. The computational domain is chosen to be large enough so that $|u| < 10^{-4}$ near the boundaries.

Instead of using the standard L^2-normalization during the iterations, we employ peak-density normalization. Specifically, at each iteration, the approximate solution is normalized as

$$u^{(n)} = \frac{n_{\max}}{\|u^{(n)}\|_\infty^2} u^{(n)} \,, \tag{17}$$

where $n_{\max}$ is a fixed constant. The iterations are stopped when the maximum of the residual of Eq. (13a) is smaller than 10^{-6}. The physical meaning of $n_{\max}$ is the peak density of the atoms in the bound state,

$$n_{\max} = \|\psi\|_\infty^2 = \|u\|_\infty^2 \,. \tag{18}$$

Unlike L^2 normalization, peak-density normalization typically converges even for unstable bound states [45], which is advantageous for our study. Consequently, as discussed below, not all these bound states are ground states in the sense of Definition (14).

5. Properties of the bound states

In this section we compute the bound states of System (13) inside the Unstable Region II using the parameters $g_1 = 1, g_2 = -1$, and with the prolate harmonic trapping potential (3) with $V_0 = 0.1$ and $\kappa = 0.25$. We do so over a wide range of peak-densities, *i.e.*, $0 < n_{\max} < 64$. Fig. 2 shows the mapping between the total number of atoms and energy of the bound states. There are two distinct – but "close" – branches, which are demarcated by a cusp point (B). The bound states in the upper branch (such as Point C) possess slightly higher energy than those in the lower branch for the same number of atoms. Therefore, the upper branch bound states are not ground states in the sense of Definition (14). The bifurcation

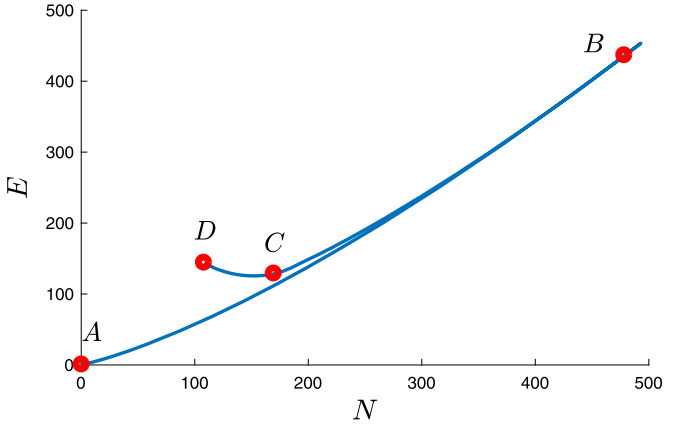

Fig. 2. Bound state energy (7) *vs.* total number of atoms (6). Points A–D designate specific values in parameter space for comparison with Figs. 5 and 6.

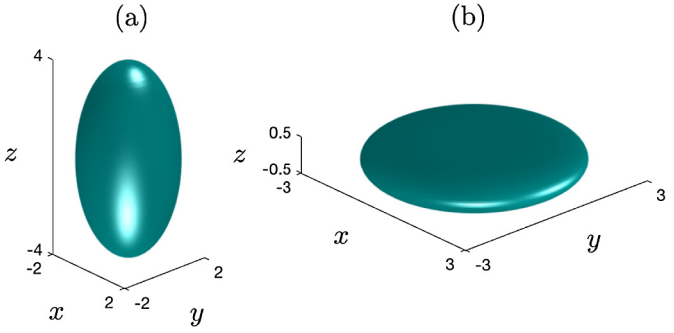

Fig. 3. Iso-surface plots of the bound states corresponding to (a) Point A and (b) Point C in Fig. 2.

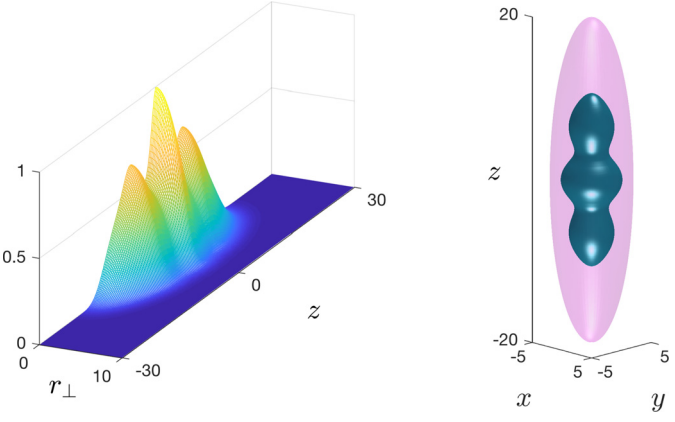

Fig. 4. Mesh plot in the $r_\perp - z$ plane and iso-surface plot of the "candlestick" bound state corresponding to the cusp point (Point B) in Fig. 2. The magenta surface delineates the trapping potential. (For interpretation of the colors in the figure(s), the reader is referred to the web version of this article.)

around the cusp point corresponds to transition in the shape of the bound states from oblate to prolate, as demonstrated in Fig. 3. For graphical purposes the solutions are plotted over the $r_\perp - z$ plane and (by rotating around the z axis) as iso-contours in 3D space.

We remark that all of these bound states are non-oscillatory. Hence, even those bound states that are not ground states in the sense of (14) are not excited states in the usual sense. In particular, Fig. 4 shows the ground state at the cusp point, which occurs at $n_{\max} = 1$. We refer to this special ground state as "candlestick" due to its central nucleus flanked by two humps. This mode is on the border between oblate and prolate bound states, though its overall structure is complex and non-spherical. For the mode, $N \approx 609$, $E \approx 619$, and $\mu \approx 1.35$. We also note that μ is determined implicitly by the choice of $n_{\max}$. The relationship between them is shown in Fig. 5. Comparing with Fig. 2 shows that the upper branch in the $N \mapsto E$ mapping has larger peak densities.

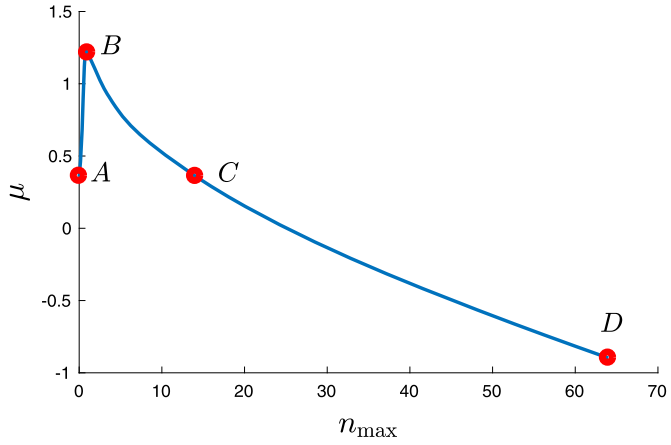

Fig. 5. Chemical potential (15) *vs.* peak density (18) for the bound states.

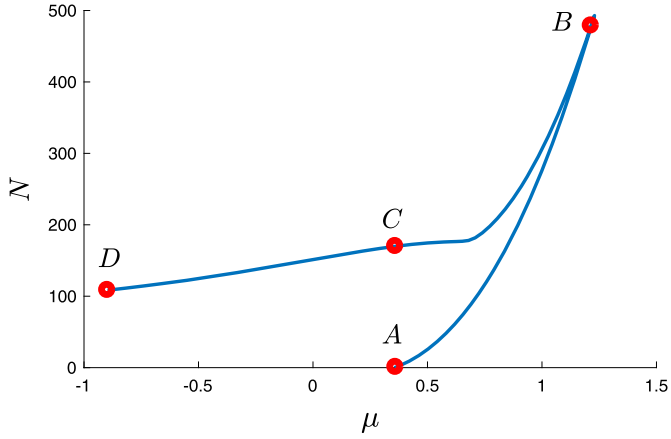

Fig. 6. Number of atoms *vs.* chemical potential for the bound states.

Fig. 6 shows the relationship between N and μ. According to the Vakhitov-Kolokolov stability criterion [47], a bound state is *linearly stable* if

$$\frac{N[u(\cdot;\mu)]}{d\mu} > 0\,. \tag{19}$$

Based on Fig. 6 the slope condition is satisfied in both branches, which indicates that all these bound states are linearly stable. We note that it is fairly common for bound states of NLS equations to be linearly (and orbitally) stable, but nonlinearly unstable [3], as we also find below.

6. Collapse dynamics

In this section we investigate the collapse dynamics in the Unstable Region II. We first recap some of the pertinent theory of peak-type collapse for isotropic NLS equations [1,3]. In particular, for the cubic NLS equation, near the collapse time, the solution can be decomposed as $\psi \sim \psi_c$ + radiation, where the collapsing part is self-similar,

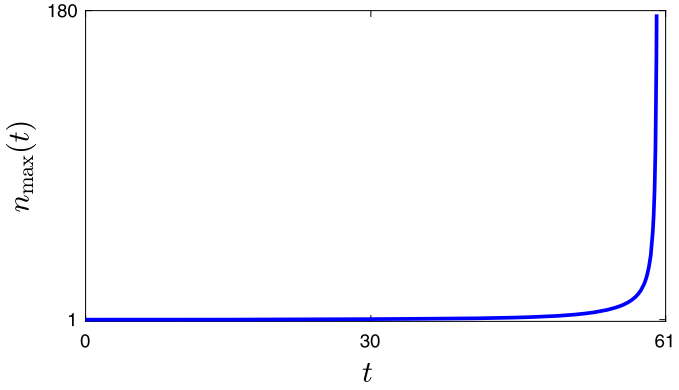

Fig. 7. Collapse of the solution of System (9) with the initial conditions (22).

$$|\psi_c|^2 \sim \frac{1}{L^2(t)} \left| Q\left(\frac{r}{L(t)}\right) \right|^2 . \tag{20}$$

Here Q is a radially-symmetric function, whose maximum is attained at the origin. $L(t)$ is the characteristic width of the collapsing part of the solution, which satisfies

$$L(t) = C\sqrt{T_c - t} , \tag{21}$$

where C is a constant that depends on the initial conditions. In the critical case ($d = 2$) this was proven rigorously by Merle and Raphael [48]. In the supercritical case ($d > 2$), the rigorous theory is much less developed, but there are many computational results that support this theory since the early studies of Zakharov et al. [4,49].

To solve System (9) we use the Split-Step technique while utilizing the axi-symmetry, quasi-discrete Hankel transform, and FFT as described above. The initial conditions are a slightly perturbed candlestick mode, *i.e.*,

$$\psi(r_\perp, z, 0) = 1.02\, u_{\rm gs}(r_\perp, z; n_{\max} = 1) . \tag{22}$$

We use the grid sizes $dr_\perp = dz \approx 0.05$ and $dt \approx 5 \cdot 10^{-4}$.

Fig. 7 shows the collapse of the peak density of the time-dependent solution[3]

$$n_{\max}(t) = \|\psi(\cdot, t)\|_\infty^2 . \tag{23}$$

To the eye, the solution remains stable up until it near the singularity time. This further indicates that this ground state being linearly stable but nonlinearly unstable. Figs. 8 and 9 show the solution at different time values. These plots show that the nucleus flattens (becomes oblate) while its peak density increases. The two humps are still there, but they remain small and do not enter the collapsing region.

To investigate this dynamics in further detail, it is useful to recover the widths of the nucleus from the numerical solution. We do this using the full-with at half-max (FWHM) along the radial and z axes, denoted by $L_r(t)$ and $L_z(t)$ respectively, which are the smallest values such that

$$|\psi(L_r, 0, t)|^2 = \frac{n_{\max}(t)}{2} , \tag{24a}$$

$$|\psi(0, L_z, t)|^2 = \frac{n_{\max}(t)}{2} . \tag{24b}$$

To check whether the collapsing nucleus is self-similar, we plot the rescaled density along the radial and axial directions, computed as

$$|\tilde{\psi}(r_\perp, 0, t)|^2 = |\psi(\xi, 0, t)|^2 / n_{\max}(t) , \tag{25a}$$

$$|\tilde{\psi}(0, z, t)|^2 = |\psi(0, \zeta, t)|^2 / n_{\max}(t) , \tag{25b}$$

where the dynamically rescaled radial and axial variables are

$$\xi(t) = \frac{r_\perp}{L_r(t)} , \qquad \zeta(t) = \frac{z}{L_z(t)} . \tag{26}$$

Fig. 10 shows the self-similar structure of the radial and axial profiles near the collapse time. In the rescaled coordinates, the two humps remain non-negligible, but appear to move away from the nucleus. However, in the non-rescaled z variable, these humps are approximately "static" (see Fig. 9) while the nucleus' width is shrinking. Comparing the rescaled profiles along the radial and axial directions, Fig. 11 shows that they appear to approach the same self-similar profile as $t \to T_c$. This suggests that the rescaled shape of the nucleus is described by a spherically-symmetric function, *i.e.*, the nucleus approaches an oblate ellipsoid.

We also plot the aspect ratio $L_r(t)/L_z(t)$ in Fig. 12 as function of $n_{\max}(t)$ to stretch the dynamics near the collapse time. The nucleus becomes gradually more oblate as its width shrinks, which further demonstrates the anisotropic nature of this collapse. Physically, this corresponds to different contraction rates along the dipole axis and perpendicular to it. It is interesting to study the rate of this collapse.

Fig. 13 shows that the radial width decreases approximately as in the isotropic case (21). In contrast, the axial width decreases linearly in time. By extrapolating $L_r(t)$ and $L_z(t)$ beyond the breakdown of the numerical solution, it appears that they both approach zero at the same time. Thus, these results suggest that near the collapse time, the widths scale as

$$L_r(t) \sim \sqrt{T_c - t} \tag{27a}$$

$$L_z(t) \sim T_c - t . \tag{27b}$$

We also recover the collapse rate using the peak-density metric

$$\ell_\infty = \frac{1}{n_{\max}(t)} . \tag{28}$$

Fig. 14 shows that this collapse rate scales approximately as

$$\ell_\infty \sim (T_c - t)^p , \quad p \approx 2 . \tag{29}$$

These results suggest that, near the collapse time, the dynamics of the nucleus (the collapsing part of the solution) is self-similar and obeys the scaling law

$$|\psi_c(\mathbf{r}, t)|^2 \sim \frac{1}{\ell_\infty(t)} |Q(\xi(t), \zeta(t))|^2 , \tag{30}$$

using the rescaled variables (26), the rates (27)–(29), and Q is a spherically symmetric function, *i.e.*,

$$Q(\xi, \zeta) = Q(\eta) , \quad \eta(t) = \sqrt{\xi^2(t) + \zeta^2(t)} . \tag{31}$$

Based on this ansatz, the total number of atoms within the collapsing region scales as

$$N[\psi_c] = \int |\psi_c(\mathbf{r}, t)|^2 d\mathbf{r} \sim \frac{2\pi}{\ell_\infty(t)} \int |Q(\xi, \zeta)|^2 L_r^2 L_z \xi d\xi d\zeta$$

$$= \frac{L_r^2(t) L_z(t)}{\ell_\infty(t)} N[Q] = C(T_c - t)^{2-p} , \tag{32}$$

for some constant C and exponent $p \approx 2$. In contrast, for peak-type collapse in the isotropic (3+1)D cubic NLS equation, the collapsing mass approaches zero ("weak collapse") at the rate $\sqrt{T_c - t}$ [3].

[3] Not to be confused with the peak density of the bound state.

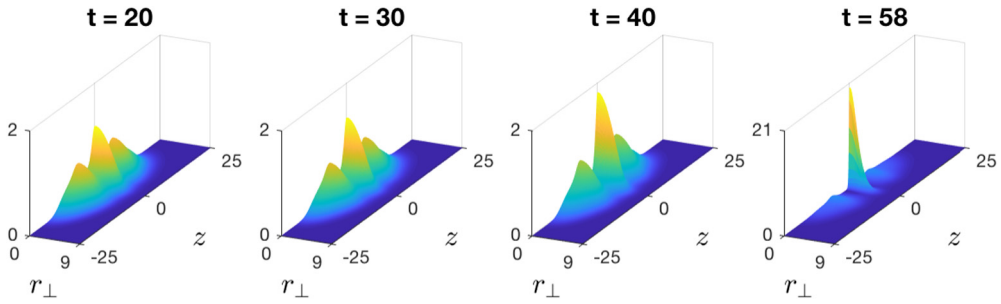

Fig. 8. Mesh plots of the solutions at different times.

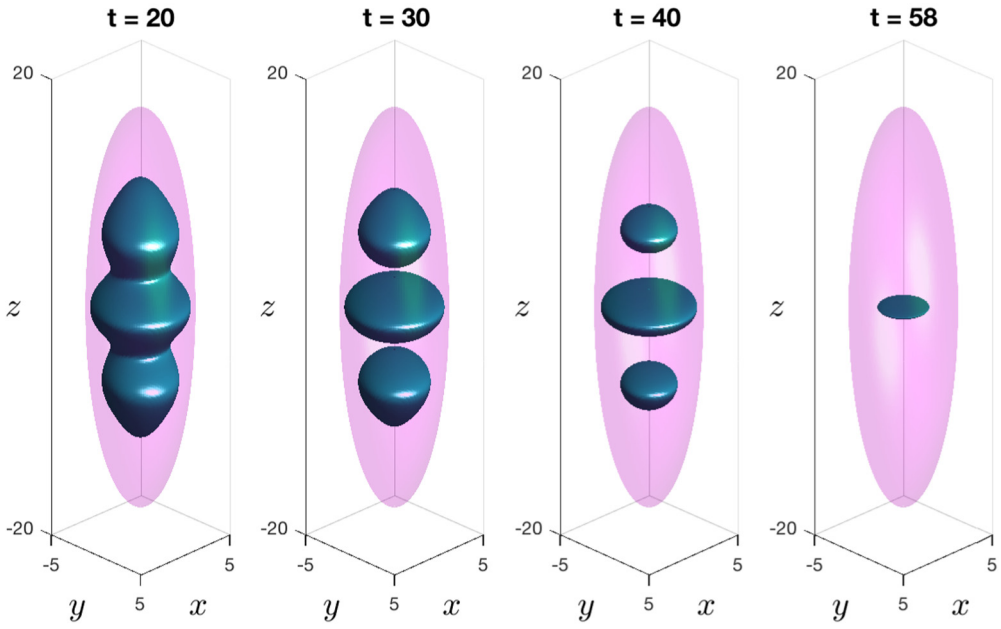

Fig. 9. Iso-surface plots corresponding to the same time values as in Fig. 8.

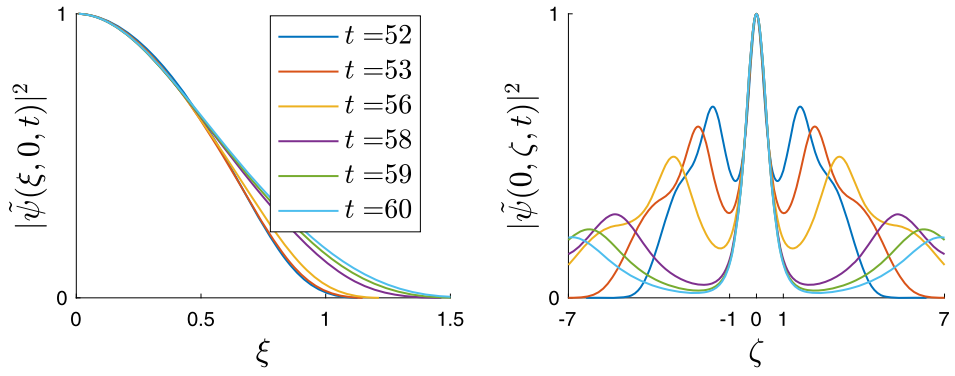

Fig. 10. Rescaled profiles of the density in the vicinity of the nucleus along the ξ and ζ axes [Eqns. (25)] at the times shown in the legend.

These results can be interpreted as follows. The attractive dipolar interactions are stronger than two-body local attractive interactions (those corresponding to a focusing cubic term). This leads to more rapid collapse, which slows down the radiation of mass from the collapsing region.

7. Dynamics at the borderline of Unstable Region II

In this section we investigate the dynamics at the borderline of Unstable Region II. To do this, we choose the parameters $g_1 = 1$ (as before) and $g_2 = -0.5$, so that $g_1 + 2g_2 = 0$. We compute the ground state with $n_{\max} = 1$ (with the same trapping potential and parameters as before), $u_1(\boldsymbol{x})$, – see Fig. 15. Here it simply takes an prolate shape ($L_z/L_r \approx 3.4$) trapped inside the prolate potential. For this bound state, $N \approx 10^3$, $E \approx 10^3$, and $\mu \approx 1.4$.

To study its nonlinear stability, the initial wavefunction is chosen as $1.1u_1(\boldsymbol{x})$. Fig. 16 shows the ensuing dynamics: the peak density undergoes bounded oscillations, while the (normalized) widths hardly change at all. This demonstrates that the condensate is nonlinearly stable for long propagation times. This result, along

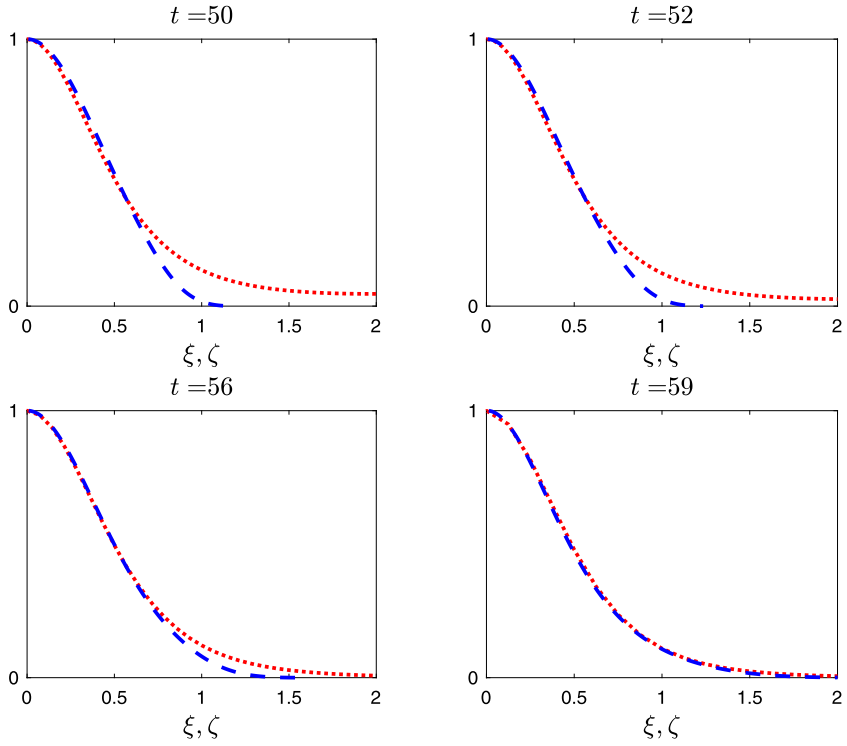

Fig. 11. Comparison of the rescaled profiles along the rescaled ξ (dashes) and ζ (dots) axes.

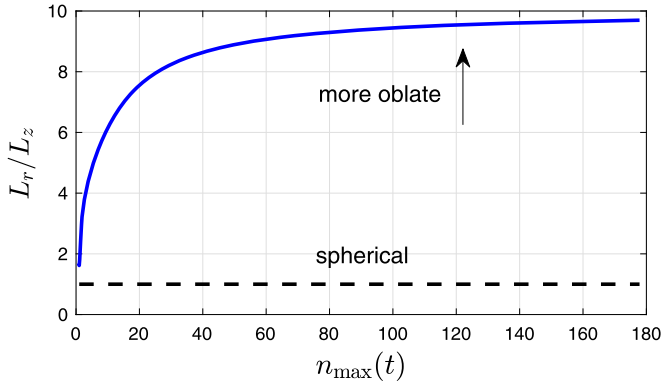

Fig. 12. Aspect ratio of the nucleus *vs.* peak density.

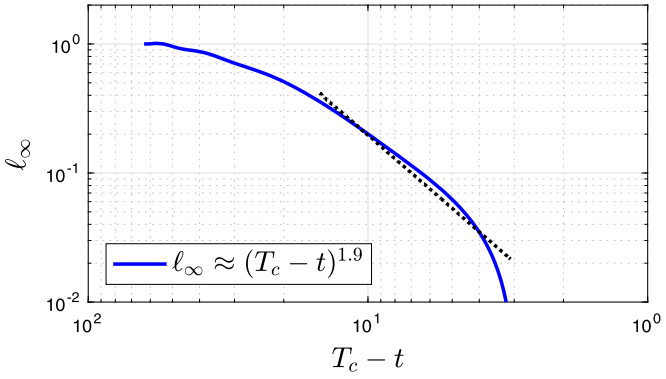

Fig. 14. Blow-up rate (28) of the peak density (log axes).

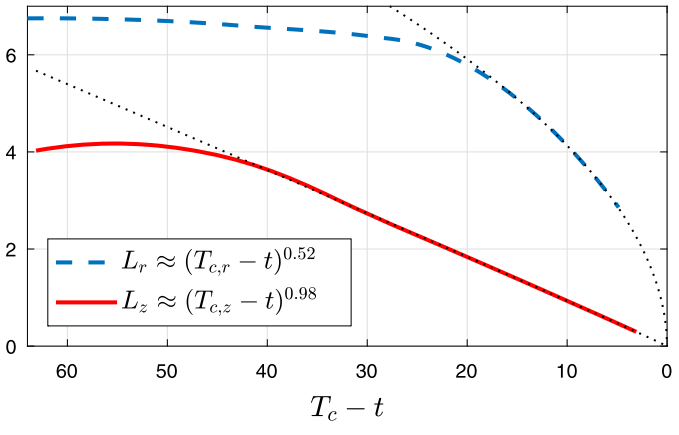

Fig. 13. Radial and axial widths of the nucleus and best power-law fits near the collapse time (dotted curves).

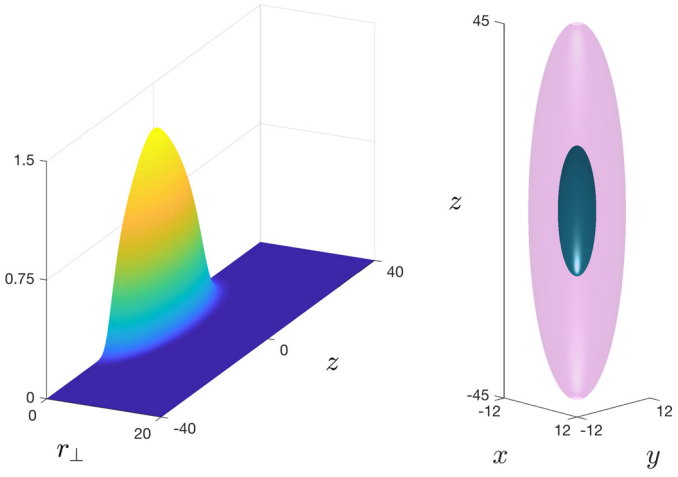

Fig. 15. Plots of the ground state with $g_1 = 1$, $g_2 = -0.5$, and $n_{\max} = 1$.

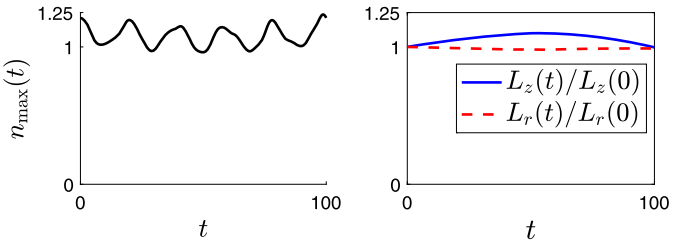

Fig. 16. Stable dynamics of the condensate's peak density (left) and normalized axial and radial widths (right).

with many other simulations we perform, indicate the criteria for Unstable Region II are at close to being sharp, in the sense that, when $g_2 < 0$ and $g_1 + 2g_2 < 0$, collapse (of an initially-perturbed bound state) can occur.

8. Conclusions

The ability to tune the signs of the short and long-range boson-boson interactions opens the door for novel many-body dynamics in BECs. In the Unstable Region II, which corresponds to sufficiently strong and attractive dipolar interactions, a family of bound states of the generalized Gross-Pitaevskii equation bifurcate from a cusp point. The candlestick (cusp-point) ground state is nonlinearly unstable and undergoes anisotropic collapse. The scaling laws of this collapse dynamics differ significantly from those of isotropic collapse. These results suggest that supercritical collapse with dipolar interactions can behave qualitatively different from the isotropic, local-nonlinearity case. Moreover, this offers new possibilities to control the dynamics of dipolar BECs.

Declaration of competing interest

The authors declare that they have no known competing financial interests or personal relationships that could have appeared to influence the work reported in this paper.

Acknowledgements

The authors would like to thank G. Fibich for useful ideas and conversations. The computations for this work were performed using the Multi-Environment Research Computer for Exploration and Discovery (MERCED) cluster.

References

[1] C. Sulem, P.L. Sulem, The Nonlinear Schrödinger Equation: Self-Focusing and Wave Collapse, Springer, 1999.
[2] J. Eggers, M.A. Fontelos, The role of self-similarity in singularities of partial differential equations, Nonlinearity 22 (1) (2008) R1.
[3] G. Fibich, The Nonlinear Schrödinger Equation: Singular Solutions and Optical Collapse, Springer, 2015.
[4] V. Zakharov, L. Shur, Self-similar regimes of wave collapse, Zh. Eksp. Teor. Fiz. 81 (1981) 2019–2031.
[5] A. Wong, P. Cheung, Three-dimensional self-collapse of Langmuir waves, Phys. Rev. Lett. 52 (14) (1984) 1222.
[6] K.D. Moll, A.L. Gaeta, G. Fibich, Self-similar optical wave collapse: observation of the Townes profile, Phys. Rev. Lett. 90 (2003) 203902.
[7] B.W. Zeff, B. Kleber, J. Fineberg, D.P. Lathrop, Singularity dynamics in curvature collapse and jet eruption on a fluid surface, Nature 403 (6768) (2000) 401.
[8] C.J. Pethick, H. Smith, Bose-Einstein Condensation in Dilute Gases, Cambridge University Press, 2008.
[9] P.G. Kevrekidis, D.J. Frantzeskakis, R. Carretero-González, Emergent Nonlinear Phenomena in Bose-Einstein Condensates: Theory and Experiment, vol. 45, Springer Science & Business Media, 2007.
[10] J.M. Gerton, D. Strekalov, I. Prodan, R.G. Hulet, Direct observation of growth and collapse of a Bose-Einstein condensate with attractive interactions, Nature 408 (6813) (2000) 692.
[11] E.A. Donley, N.R. Claussen, S.L. Cornish, J.L. Roberts, E.A. Cornell, C.E. Wieman, Dynamics of collapsing and exploding Bose-Einstein condensates, Nature 412 (6844) (2001) 295.
[12] J.L. Roberts, N.R. Claussen, S.L. Cornish, E.A. Donley, E.A. Cornell, C.E. Wieman, Controlled collapse of a Bose-Einstein condensate, Phys. Rev. Lett. 86 (19) (2001) 4211.
[13] L.M. Widrow, N. Kaiser, Using the Schrödinger equation to simulate collisionless matter, Astrophys. J. 416 (1993) L71.
[14] S.-J. Sin, Late-time phase transition and the galactic halo as a Bose liquid, Phys. Rev. D 50 (6) (1994) 3650.
[15] C. Eigen, A.L. Gaunt, A. Suleymanzade, N. Navon, Z. Hadzibabic, R.P. Smith, Observation of weak collapse in a Bose-Einstein condensate, Phys. Rev. X 6 (4) (2016) 041058.
[16] T. Koch, T. Lahaye, J. Metz, B. Fröhlich, A. Griesmaier, T. Pfau, Stabilization of a purely dipolar quantum gas against collapse, Nat. Phys. 4 (3) (2008) 218.
[17] T. Lahaye, J. Metz, B. Froehlich, T. Koch, M. Meister, A. Griesmaier, T. Pfau, H. Saito, Y. Kawaguchi, M. Ueda, d-Wave collapse and explosion of a dipolar Bose-Einstein condensate, Phys. Rev. Lett. 101 (8) (2008) 080401.
[18] K. Aikawa, A. Frisch, M. Mark, S. Baier, A. Rietzler, R. Grimm, F. Ferlaino, Bose-Einstein condensation of erbium, Phys. Rev. Lett. 108 (21) (2012) 210401.
[19] S. Giovanazzi, A. Görlitz, T. Pfau, Tuning the dipolar interaction in quantum gases, Phys. Rev. Lett. 89 (13) (2002) 130401.
[20] D. Benney, G. Roskes, Wave instabilities, Stud. Appl. Math. 48 (4) (1969) 377–385.
[21] A. Davey, K. Stewartson, On three-dimensional packets of surface waves, Proc. R. Soc. Lond. Ser. A, Math. Phys. Sci. 338 (1613) (1974) 101–110.
[22] M.J. Ablowitz, İ. Bakırtaş, B. Ilan, Wave collapse in a class of nonlocal nonlinear Schrödinger equations, Physica D 207 (2005) 230–253.
[23] P.M. Lushnikov, Collapse of Bose-Einstein condensates with dipole-dipole interactions, Phys. Rev. A 66 (5) (2002) 051601.
[24] P.M. Lushnikov, Collapse and stable self-trapping for Bose-Einstein condensates with $1/r^b$-type attractive interatomic interaction potential, Phys. Rev. A 82 (2) (2010) 023615.
[25] R. Carles, P.A. Markowich, C. Sparber, On the Gross-Pitaevskii equation for trapped dipolar quantum gases, Nonlinearity 21 (11) (2008) 2569.
[26] P. Antonelli, C. Sparber, Existence of solitary waves in dipolar quantum gases, Phys. D: Nonlinear Phenom. 240 (4–5) (2011) 426–431.
[27] T. Cazenave, Semilinear Schrodinger Equations, vol. 10, American Mathematical Soc., 2003.
[28] R. Carles, H. Hajaiej, Complementary study of the standing wave solutions of the Gross-Pitaevskii equation in dipolar quantum gases, Bull. Lond. Math. Soc. 47 (3) (2015) 509–518.
[29] J. Bellazzini, L. Jeanjean, On dipolar quantum gases in the unstable regime, SIAM J. Math. Anal. 48 (3) (2016) 2028–2058.
[30] G. Fibich, B. Ilan, S. Schochet, Critical exponents and collapse of nonlinear Schrödinger equations with anisotropic fourth-order dispersion, Nonlinearity 16 (5) (2003) 1809.
[31] G. Fibich, N. Gavish, X.-P. Wang, New singular solutions of the nonlinear Schrödinger equation, Phys. D: Nonlinear Phenom. 211 (3–4) (2005) 193–220.
[32] S. Yi, L. You, Trapped condensates of atoms with dipole interactions, Phys. Rev. A 63 (5) (2001) 053607.
[33] P. Pedri, L. Santos, Two-dimensional bright solitons in dipolar Bose-Einstein condensates, Phys. Rev. Lett. 95 (20) (2005) 200404.
[34] I. Tikhonenkov, B. Malomed, A. Vardi, Anisotropic solitons in dipolar Bose-Einstein condensates, Phys. Rev. Lett. 100 (9) (2008) 090406.
[35] I. Tikhonenkov, B. Malomed, A. Vardi, Vortex solitons in dipolar Bose-Einstein condensates, Phys. Rev. A 78 (4) (2008) 043614.
[36] S. Rau, J. Main, H. Cartarius, P. Köberle, G. Wunner, Variational methods with coupled Gaussian functions for Bose-Einstein condensates with long-range interactions. II. Applications, Phys. Rev. A 82 (2) (2010) 023611.
[37] M.A. Baranov, Theoretical progress in many-body physics with ultracold dipolar gases, Phys. Rep. 464 (3) (2008) 71–111.
[38] T. Lahaye, C. Menotti, L. Santos, M. Lewenstein, T. Pfau, The physics of dipolar bosonic quantum gases, Rep. Prog. Phys. 72 (12) (2009) 126401.
[39] R.M. Wilson, S. Ronen, J.L. Bohn, Angular collapse of dipolar Bose-Einstein condensates, Phys. Rev. A 80 (2) (2009) 023614.
[40] P. Köberle, D. Zajec, G. Wunner, B.A. Malomed, Creating two-dimensional bright solitons in dipolar Bose-Einstein condensates, Phys. Rev. A 85 (2) (2012) 023630.
[41] D. Edler, C. Mishra, F. Wächtler, R. Nath, S. Sinha, L. Santos, Quantum fluctuations in quasi-one-dimensional dipolar Bose-Einstein condensates, Phys. Rev. Lett. 119 (5) (2017) 050403.
[42] W. Bao, Y. Cai, H. Wang, Efficient numerical methods for computing ground states and dynamics of dipolar Bose-Einstein condensates, J. Comput. Phys. 229 (20) (2010) 7874–7892.
[43] W. Bao, S. Jiang, Q. Tang, Y. Zhang, Computing the ground state and dynamics of the nonlinear Schrödinger equation with nonlocal interactions via the nonuniform FFT, J. Comput. Phys. 296 (2015) 72–89.
[44] W. Bao, Q. Tang, Y. Zhang, Accurate and efficient numerical methods for computing ground states and dynamics of dipolar Bose-Einstein condensates via the nonuniform FFT, Commun. Comput. Phys. 19 (5) (2016) 1141–1166.

[45] J. Yang, T.I. Lakoba, Accelerated imaginary-time evolution methods for the computation of solitary waves, Stud. Appl. Math. 120 (3) (2008) 265–292.
[46] M. Guizar-Sicairos, J.C. Gutiérrez-Vega, Computation of quasi-discrete Hankel transforms of integer order for propagating optical wave fields, J. Opt. Soc. Am. A 21 (1) (2004) 53–58.
[47] M.G. Vakhitov, A.A. Kolokolov, Stationary solutions of the wave equation in a medium with nonlinearity saturation, Radiophys. Quantum Electron. 16 (1973) 783–798.
[48] F. Merle, P. Raphael, On universality of blow-up profile for L^2 critical nonlinear Schrödinger equation, Invent. Math. 156 (3) (2004) 565–672.
[49] V. Zakharov, Collapse and self-focusing of Langmuir waves, in: Basic Plasma Physics: Selected Chapters, Handbook of Plasma Physics, vol. 1, 1983, p. 419.